

Article

Mechanically Strong CaSiO_3 Scaffolds Incorporating B_2O_3 -ZnO Liquid Phase

Cijun Shuai ^{1,2,3}, Songlin Duan ¹, Dan Gao ⁴, Ping Wu ⁵, Chengde Gao ¹, Youwen Yang ¹, Long Liu ¹, Fulai Yuan ⁶, Sheng Yang ^{7,*} and Pei Feng ^{1,*}

¹ State Key Laboratory of High Performance Complex Manufacturing, Central South University, Changsha 410083, China; shuai@csu.edu.cn (C.S.); airyflier@csu.edu.cn (S.D.); gaochengde@csu.edu.cn (C.G.); yangyouwen@csu.edu.cn (Y.Y.); liulong@csu.edu.cn (L.L.)

² State Key Laboratory for Powder Metallurgy, Central South University, Changsha 410083, China

³ State Key Laboratory of Solidification Processing, Northwestern Polytechnical University, Xi'an 710072, China

⁴ Key Laboratory of Carcinogenesis of the Chinese Ministry of Health, Xiangya Hospital, Central South University, Changsha 410083, China; gd146611004@csu.edu.cn

⁵ College of Chemistry, Xiangtan University, Xiangtan 411105, China; pingwu@xtu.edu.cn

⁶ Health Management Center, Xiangya Hospital, Central South University, Changsha 410008, China; fulaiyuan2010@163.com

⁷ Human Reproduction Center, Shenzhen Hospital of Hongkong University, Shenzhen 518053, China

* Correspondence: tobyys2000@aliyun.com (S.Y.); fengpei@csu.edu.cn (P.F.); Tel.: +86-755-8691-3333 (S.Y.); +86-731-8887-9044 (P.F.)

Academic Editor: Peter Van Puyvelde

Received: 7 March 2017; Accepted: 11 April 2017; Published: 13 April 2017

Abstract: Calcium silicate (CaSiO_3) scaffolds were reinforced by introducing liquid phase. The liquid phase was made of B_2O_3 and ZnO. The fracture toughness and compressive strength increased by 48% and 141%, respectively, compared with those of the scaffolds without the liquid phase. This was attributed to the enhanced densification, the elongated grains pull-out and the cracks bridging. In addition, because of its increasing mechanical properties, the fracture model of the cleavage fracture was more beneficial than the intergranular fracture. The mechanical properties of the scaffolds with the liquid phase could be steadily maintained and then they decreased slowly when immersed in simulated body fluid (SBF). Meanwhile, the hydroxyapatite (HAp) generated on their surfaces. In addition, the scaffolds possessed favorable biocompatibility and could promote cell proliferation. These results demonstrated that the scaffolds with B_2O_3 -ZnO liquid phase are a promising substitute for bone repair applications.

Keywords: CaSiO_3 scaffolds; liquid phase; selective laser sintering; mechanical properties

1. Introduction

Bioactive ceramics, such as bioglasses, hydroxyapatite (HAp) and calcium silicate (CaSiO_3), are accepted as the most promising bone implant substitutes in bone tissue engineering [1–3]. Recently, CaSiO_3 has attracted increasing attention due to its excellent HAp-forming ability and outstanding proliferation ability of osteoblast-like cells [4,5]. However, its inherent brittleness causes an insufficient mechanical strength that makes it hardly able to provide structural support for the new bone ingrowth, which impedes its clinical application in load-bearing bone repair [6,7].

Some methods, such as second-phase enhancement and liquid phase sintering (LPS), are effective at enhancing the mechanical properties of ceramics. Nevertheless, incorporation of second-phase materials into ceramics, e.g., silicon carbide (SiC) [8], zirconia (ZrO_2) [9], aluminium oxide (Al_2O_3) [10], silver oxide (Ag_2O) [11] and titanium oxide (TiO_2) [12,13], makes it hard to acquire sufficient

mechanical strength to satisfy the demand of load-bearing bone replacement. LPS is an approach that aims to rapidly achieve a dense ceramic with a high mechanical strength [14,15].

Diboron trioxide (B_2O_3) is a well-known liquid facilitator has been frequently used to decrease the sintering temperature and modify the densification of ceramics [16–18]. Yang et al. incorporated B_2O_3 into a $CaO-SiO_2-P_2O_5$ system to form liquid phase and improve the strength of glass ceramics by electric furnace sintering [19]. Wang et al. pointed out that B_2O_3 -containing bioglass could distinctly reinforce mechanical strength of akermanite ceramics as liquid phase via pressureless sintering [18]. Moreover, boron has a stimulatory effect on increasing extracellular matrix turnover, wound healing and bone physiology [20,21]. Besides, zinc has well-defined biological roles. It can stimulate bone formation, promote osteoblastic cells proliferation and inhibit osteoclastic bone resorption [22–24].

In this study, B_2O_3 -ZnO liquid phase system was developed according to their phase diagram and then they were incorporated in $CaSiO_3$ powder. The porous architectures of the scaffolds were established using selective laser sintering (SLS). The study focused on the microstructure evolutions and reinforcement behaviors of the scaffolds with the liquid phase. Moreover, the influences of the liquid phase on the biodegradability, bioactivity and biocompatibility of the scaffolds were also investigated.

2. Experimental Procedure

2.1. Materials and Processing

$CaSiO_3$ powder was obtained from Kunshan Huaqiao New Materials Co. Ltd. (Kunshan, China). ZnO powder (99.9% purity) and B_2O_3 powder (99.999% purity) were purchased from Hefei Aijia New Materials Technology Co. Ltd. (Hefei, China) and Alfa Aesar Co., Ltd. (Shanghai, China), respectively.

In the phase diagram of B_2O_3 and ZnO [25], there was a eutectic zone at the mole ratio of B_2O_3 to ZnO from 1:1 to 2:5 (weight ratios: from 47:53 to 25:75). The lowest eutectic temperature appeared at the mole ratio of 2:3 (weight ratio: 35:65). In the study, several proportions at the range were chosen to prepare liquid phase (Table 1). Initially, the B_2O_3 and ZnO powders were mixed and then dispersed using ball-milling for 4 h in ethanol media followed by drying at 70 °C for 24 h. Finally, 3 wt % of the mixed powders were incorporated into $CaSiO_3$ powder followed by ball-milling for 24 h to prepare ternary powders.

Table 1. $CaSiO_3$ scaffolds with B_2O_3 -ZnO liquid phase at different compositions.

Group	Compositions of Scaffolds		Compositions of Liquid Phase	
	$CaSiO_3$ (wt %)	Liquid Phase (wt %)	B_2O_3 (wt %)	ZnO (wt %)
CS	100	0	0	0
CS-A	97	3	47	53
CS-B	97	3	40	60
CS-C	97	3	35	65
CS-D	97	3	25	75

Porous scaffolds were constructed layer-by-layer using a homemade SLS equipment [26]. The sintering parameters were kept constant as follows: layer thickness of 0.12 mm and the laser power (1 mm focused beam diameter) of 7 W and scan speed of 100 mm/min. When the sintering was complete, the scaffolds were obtained after brushing off unsintered powder.

2.2. Physical and Chemical Properties Characterization

The microstructure of the initial powders and scaffolds was examined using scanning electron microscope (SEM; Tescan Mira3 LMU, Brno, Czech) with accelerating voltage of 20 kV after sputtering with a thin platinum film. The chemical composition was analyzed using energy dispersive spectroscopy (EDS; Oxford X-Max20, Oxford, UK), X-ray diffraction (XRD; Rigaku D/Max 2550,

Tokyo, Japan) with CuK α radiation at 40 kV/250 mA and scanning rate of 8 degree/min, and Fourier transform infrared spectroscopy (FTIR; Nicolet 6700, Madison, WI, USA) with a resolution of 8 cm⁻¹ and the range of 4000–400 cm⁻¹.

2.3. Mechanical Properties Assessment

Vickers hardness of the scaffolds was measured with an indentation hardness tester (HXD-1000TM/LCD, Shanghai, China). Six indentations were recorded at an indentation load of 300 gf and a dwelling time of 10 s to determine the Vickers hardness. Simultaneously, the length of induced crack was used to calculate fracture toughness (K_{IC} , MPa·m^{1/2}) according to the Equation (1) [27]:

$$K_{IC} = 0.0824 (P/c^{3/2}) \quad (1)$$

where P is the indentation load (N) and c is the induced crack radius length (m).

Compressive strength tests were carried out on a computer-controlled desktop universal tester (WD-D1, Shanghai, China) at a cross-head speed of 0.5 mm/min. Compressive strength of the scaffolds was confirmed according to stress-strain curve. Six scaffolds of each group were utilized to perform this experiment. The results were presented as means \pm standard deviation (SD).

2.4. Bioactivity and Biodegradability Assessment

The bioactivity and biodegradability of the scaffolds were evaluated by immersing in simulated body fluid (SBF) [28]. The scaffolds (W_0) were exposed to SBF solution for different periods (3, 7, 14, 21 and 28 days) with the liquid/solid ratio of 100 mL/g. The immersion experiments were carried out at 37 °C and the SBF solution were renovated every two days. At each time point, the scaffolds were taken out, rinsed with distilled water and dried at 60 °C for 24 h. Once dried, the weight was carefully measured and recorded (W_t). The weight loss was calculated according to the Equation (2). Then, the formation of HAp on the scaffolds was characterized by SEM and FTIR. The compressive strength of the scaffolds was measured after soaking.

$$\text{Weight loss} = (W_t - W_0)/W_0 \times 100\% \quad (2)$$

2.5. Cytocompatibility and Cell Viability Assessment

Cell culture experiments were performed on the scaffolds to evaluate cytocompatibility and cell viability. The scaffolds were autoclaved at 121 °C for 40 min. Subsequently, they were rinsed with aseptic phosphate buffered saline (PBS), pre-wetted with Dulbecco's Modified Eagle's Medium (DMEM) and then placed in 12-well plates. Osteoblast-like cells (MG-63) were seeded on the scaffolds at a density of 4×10^4 cells per well. Incubations were run in DMEM supplemented with 10% fetal bovine serum (FBS) and 1% streptomycin/penicillin at 37 °C under a 5% CO₂ humidified atmosphere. The culture medium was changed every day for the duration of the experiment.

Cell proliferation was quantitative estimated by 3-(4,5-dimethylthiazol-2-yl)-2,5-diphenyl tetrazolium bromide (MTT) assay. After cultivating for 3 days, MTT, a yellow tetrazolium salt, was diluted in DMEM and added to each well to form a purple formazan due to an enzymatic reaction by the living cell. After culturing for a further 4 h, dimethyl sulfoxide was blended to all wells to entirely resolve the purple formazan. Absorbance of each well at 490 nm was confirmed on a microplate reader ($n = 3$).

Cell viability was also qualitatively assessed by examining cells' attachment and spreading behaviors. The scaffolds were washed twice gently with PBS after incubating for 1, 2 and 3 days, and then fixed with 2.5% glutaraldehyde aqueous solution for 2 h and dehydrated twice in a series of ethanol solutions (70%, 80%, 90%, 95% and 100%), respectively. Afterward, the scaffolds were dried and coated with platinum, and then observed under SEM.

3. Results and Discussion

3.1. Sintering Behavior

The XRD patterns and morphology of the received powders were presented in Figure 1. Compared with the standard XRD patterns of CaSiO_3 (beta phase, JCPDS 84-0654) and ZnO (JCPDS 36-1451), it was clear that all of the primary strong and sharp diffraction peaks of the CaSiO_3 (Figure 1a) and ZnO (Figure 1b) powders could be indexed, respectively. The B_2O_3 powder was amorphous which was identified completely by the B_2O_3 diffraction code of JCPDS 06-0297 (Figure 1c). CaSiO_3 and B_2O_3 powders had a particle-like morphology with an average particle size of $1.5 \mu\text{m}$ and $40 \mu\text{m}$ respectively, and ZnO had a whisker-like shape. The rhomboid scaffolds had a 75-degree acute angle and dimensions of $14 \times 14 \times 5 \text{ mm}^3$ (length \times width \times height) (Figure 1d). Other researchers reported that scaffolds required a pore size greater than $300 \mu\text{m}$ to promote vascularisation and bone ingrowth for bone repair [29,30]. The struts and pores of the scaffolds were around 2 mm and 1 mm, respectively. Moreover, the external and internal architectures of the scaffolds were well controlled.

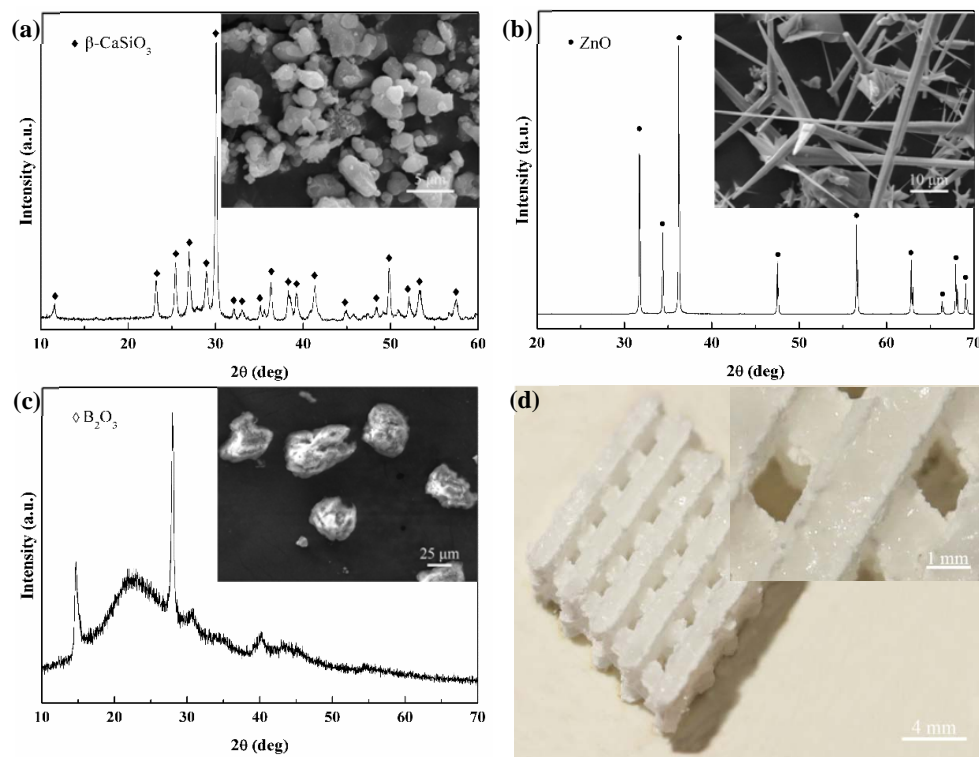


Figure 1. X-ray diffraction (XRD) patterns and microstructures of (a) CaSiO_3 powder; (b) ZnO powder and (c) B_2O_3 powder and (d) a CaSiO_3 scaffold (enlarged image at top right corner).

The diffraction peaks of all scaffolds were similar and no new phases were detected (Figure 2). Compared with the standard patterns of beta CaSiO_3 and alpha CaSiO_3 (JCPDS 74-0874), the two phases existed in all patterns, which represented a certain extent of phase transformation from beta phase to alpha phase during the sintering process. These results indicated that B_2O_3 - ZnO liquid phase did not react with CaSiO_3 .

Microstructures of the thermally etched surface at $1050 \text{ }^\circ\text{C}$ in air were displayed in Figure 3. The group CS, CS-A, CS-B, CS-C and CS-D represented the CaSiO_3 scaffolds without B_2O_3 - ZnO , CaSiO_3 with 47% B_2O_3 -53% ZnO , CaSiO_3 with 40% B_2O_3 -60% ZnO , CaSiO_3 with 35% B_2O_3 -65% ZnO and CaSiO_3 with 25% B_2O_3 -75% ZnO , respectively. The grains were arranged loosely in group CS and there were some holes, which demonstrated that densification was not sufficient for the scaffolds

without liquid phase (Figure 3a). The other four groups revealed a highly dense structure, which indicated that the liquid phase enhanced sinterability and densification. Group CS-A (Figure 3b) possessed a relatively uniform particle size. In groups CS-B (Figure 3c) and CS-C (Figure 3d), several elongated grains appeared because the CaSiO_3 grains grew rapidly along the non-uniform grain morphology. Meanwhile, the space between grains of group CS-C decreased compared with group CS-B. The chemical component of group CS-C was detected by elemental maps (Figure 3f–h). The results revealed that almost all of the Zn presented in the grain boundaries (Figure 3h). Abnormal grain growth appeared at group CS-D (Figure 3e).

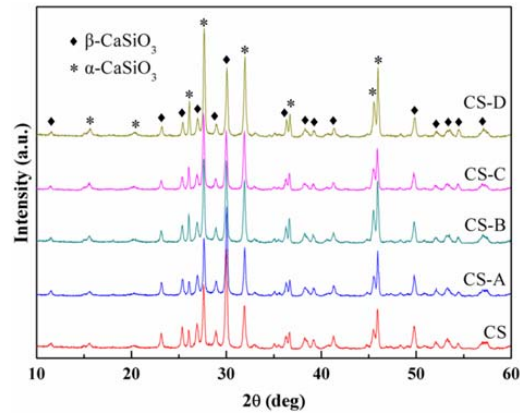


Figure 2. XRD patterns for the CaSiO_3 scaffolds.

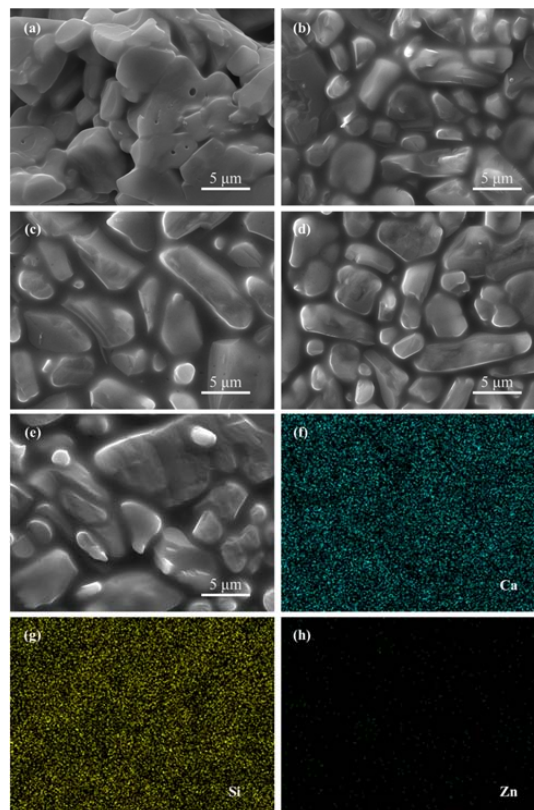


Figure 3. Microstructures of the scaffolds for groups: (a) CS; (b) CS-A; (c) CS-B; (d) CS-C and (e) CS-D; elemental maps of (f) Ca element; (g) Si element and (h) Zn element for (d).

3.2. Mechanical Properties

It is a great challenge to improve the fracture toughness and compressive strength of bioactive ceramics. The fracture toughness and compressive strength increased at first and then decreased, and the hardness gradually increased from group CS-A to CA-D (Table 2). A peak value of the fracture toughness and compressive strength appeared at group CS-C. In detail, the fracture toughness and compressive strength reached $1.57 \pm 0.15 \text{ MPa}\cdot\text{m}^{1/2}$ and $40.69 \pm 1.54 \text{ MPa}$, which increased by 48% and 141% compared with those of the scaffolds without liquid phase, respectively. This could be explained as follows: On the one hand, the mechanical properties of the scaffolds were connected with their densification. The densification of the scaffolds with the liquid phase was increased compared with the scaffolds without liquid phase (Figure 4), which improved the mechanical properties. On the other hand, the appropriate liquid phase (white arrows) that existed in grain boundary (group CS-C) could make the grains bond strong (Figure 4d), while excessive liquid phase formed a reticulate structure (group CS-A) and led to a relatively low mechanical property (Figure 4b). Moreover, the cleavage fracture (white boxes in Figure 4d) was more beneficial at improving mechanical properties than the intergranular fracture. The elongated grains pull-out and cracks bridging were also useful in enhancing the toughness (Figure 5). However, abnormal grain growth and completely intergranular fracture (group CS-D) resulted in a decrease of mechanical properties (Figure 4e).

Table 2. Effects of $\text{B}_2\text{O}_3\text{-ZnO}$ liquid phase on the hardness, fracture toughness and compressive strength.

Group	CS	CS-A	CS-B	CS-C	CS-D
Hardness (GPa)	4.95 ± 0.51	5.54 ± 0.46	6.03 ± 0.29	6.57 ± 0.39	6.71 ± 0.47
Fracture toughness ($\text{MPa}\cdot\text{m}^{1/2}$)	1.06 ± 0.12	1.214 ± 0.18	1.46 ± 0.14	1.57 ± 0.15	1.56 ± 0.13
Compressive strength (MPa)	21.82 ± 1.67	40.75 ± 1.46	47.09 ± 2.16	52.69 ± 1.54	49.97 ± 2.21

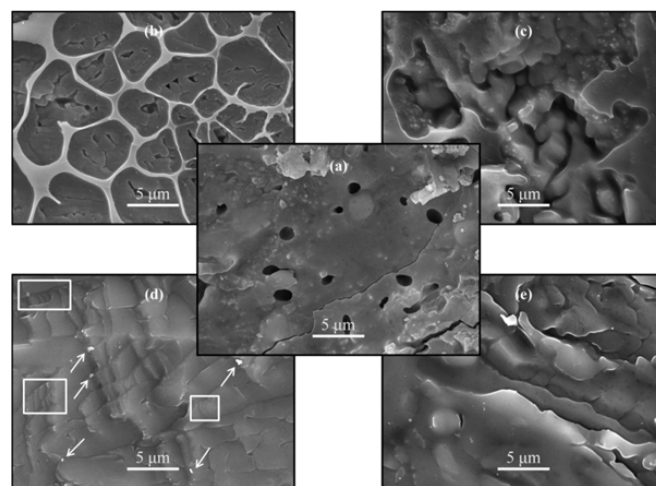


Figure 4. Fracture surfaces of the scaffolds for groups: (a) CS; (b) CS-A; (c) CS-B; (d) CS-C and (e) CS-D.

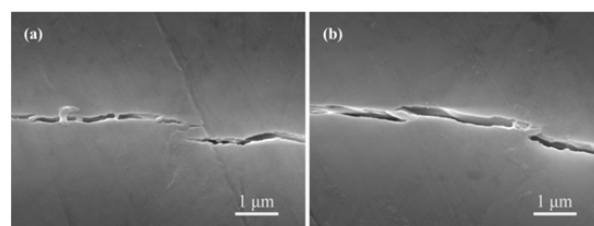


Figure 5. Toughening mechanisms for group CS-C: (a) grains pull-out and (b) crack bridging.

3.3. Bioactivity and Biodegradability

The bioactivity and biodegradability of the scaffolds were assessed. After soaking for 3 days, some granular HAp generated on the scaffolds of all groups (Figure 6). Particularly, HAp almost covered the whole scaffolds with the liquid phase, which indicated that the liquid phase improved the HAp formation ability (Figure 6b–e).

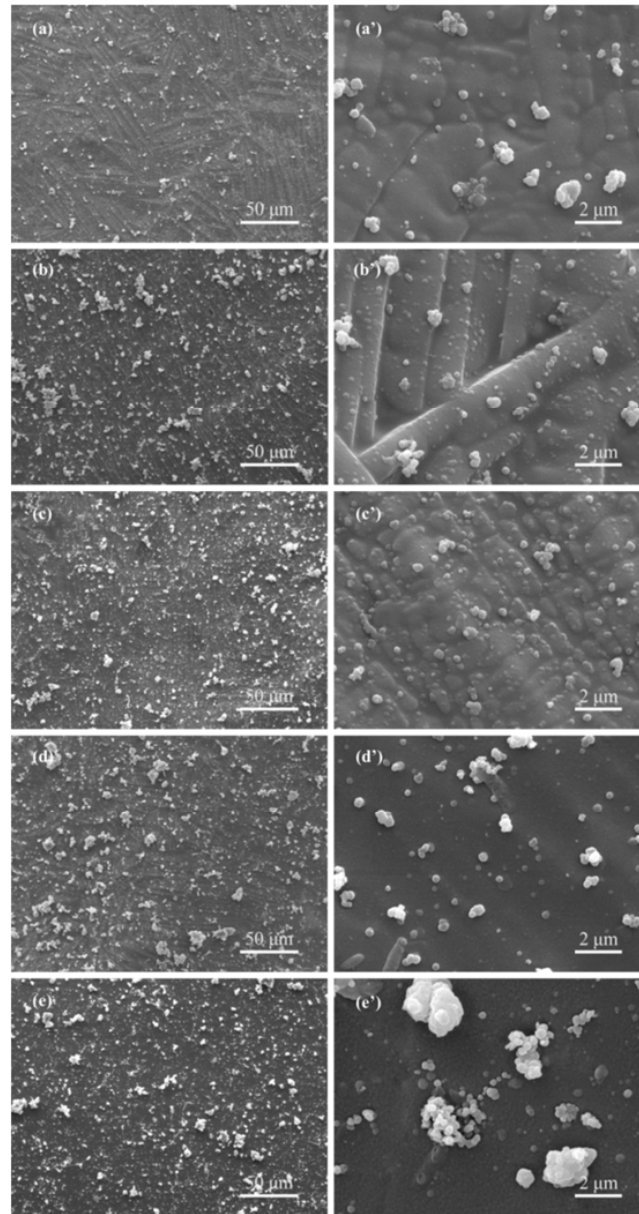


Figure 6. Morphologies for groups: (a,a') CS; (b,b') CS-A; (c,c') CS-B; (d,d') CS-C and (e,e') CS-D after immersion for 3 days.

FTIR was performed on group CS-C after immersion for different periods to further study the bioactivity (Figure 7). The absorption bands of silicate group were intense before immersing (0 day). In detail, the absorption bands were recorded at 473 and 794 cm^{-1} corresponding to the Si-O-Si vibration and the absorption bands between 922 and 985 cm^{-1} corresponded to the Si-O⁻ vibration [15,31]. After immersing, new absorption bands at 1063 and 540–605 cm^{-1} were assigned to the phosphate group (PO_4^{3-}), the absorption bands at 1400 cm^{-1} were assigned to the carbonate

group (CO_3^{2-}), and the bands at 3440 and 1635 cm^{-1} corresponded to the O-H absorption [15,31,32]. The intensity of silicate group absorption bands were evidently weakened with increasing immersion time. These results further confirmed that there was HAp on the scaffolds after immersing.

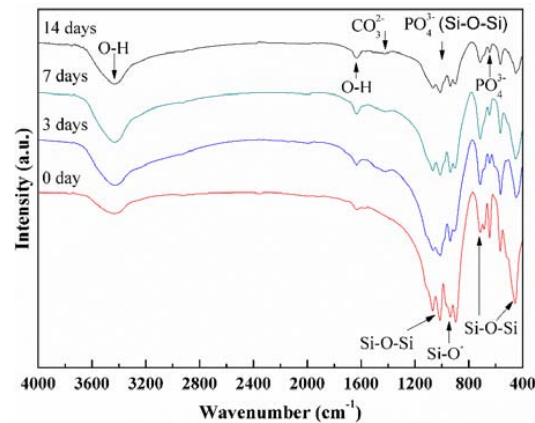


Figure 7. Fourier transform infrared spectroscopy (FTIR) spectrums of group CS-C scaffolds after immersion for 0, 3, 7 and 14 days.

The formation mechanism of HAp on scaffolds could be described as follows: When the scaffolds were immersed in the SBF, Ca^{2+} in CaSiO_3 firstly exchanged with H^+ in SBF solution giving rise to the formation of silanol (Si-OH) on the surface of the scaffolds. Thereby, a negatively charged surface with the functional group (Si-O⁻) was formed on the scaffolds. Eventually, Ca^{2+} in SBF was attracted to the scaffolds-SBF interface to form a nucleation of HAp. Once the nuclei of HAp were formed, the HAp could grow spontaneously by incorporation of Ca^{2+} and HPO_4^{2-} from the SBF.

The biodegradability of the scaffolds was evaluated by measuring the weight loss (wt %) before and after immersing experiments. Obviously, the weight loss increased with the immersing time (Figure 8a). After immersing for 28 days, the weight loss was 27% for group CS-C, which was lower than that of the scaffolds without liquid phase (41%). This was attributed to the dense structure and the inhibiting effect of the liquid phase on the CaSiO_3 grains. Meanwhile, the compressive strength of the scaffolds with the liquid phase maintained a significant increase in the first 14 days (Figure 8b). This was primarily ascribed to HAp mineralization. After immersion for 21 days, the strength decreased slightly. Therefore, the scaffolds with the liquid phase could maintain mechanical reliability and structural stability for bone repair.

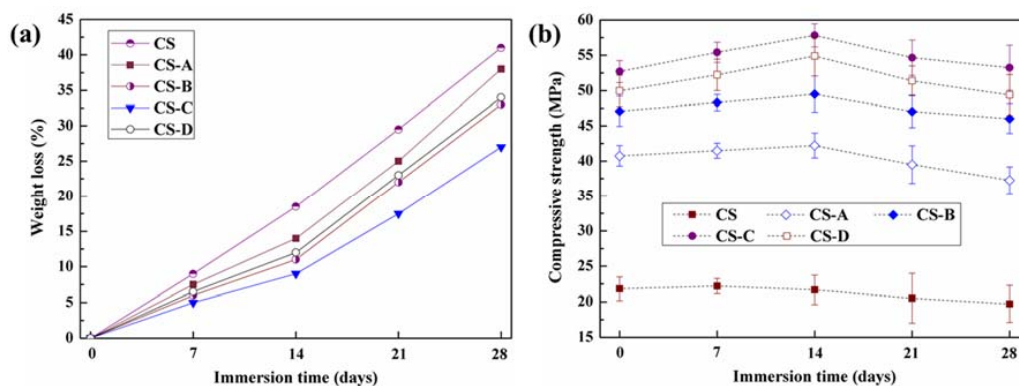


Figure 8. (a) Weight loss and (b) change of compressive strength of the scaffolds after immersing for various time periods.

3.4. Cytocompatibility and Cell Viability

The cell viability on the scaffolds underwent quantification analysis by MTT after culturing for 3 days (Figure 9). The cells proliferated more actively in groups CS-B and CS-C than other groups and reached a maximum value in group CS-C, which indicated that this group was more advantageous for cell growth than others.

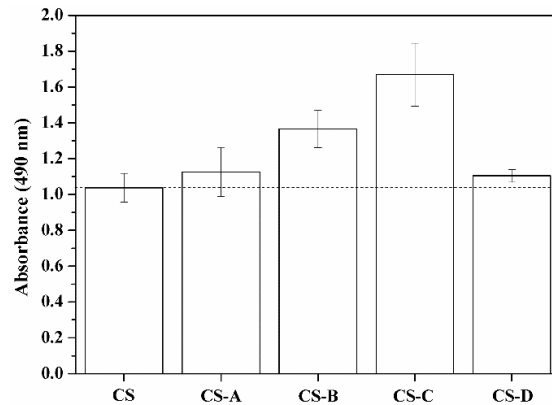


Figure 9. Cell proliferation on the scaffolds for 3 days.

The cell adhesion and spreading experiments on group CS-C indicated that the cell growth included three main stages (Figure 10). Firstly, attachment: at this stage, cells were still spherical morphology and no filopodia (Figure 10a); secondly, partly spreading: cells started to extend locally and connect by filopodia. Besides, a small quantity of the extracellular matrix was synthesized and secreted by cells (Figure 10b); lastly, spreading and flattening: the cells spread completely and connected with each other (Figure 10c). These results indicated that the cells attached on the scaffolds by means of filopodia and changed their morphologies to contact with the cell-scaffold interface.

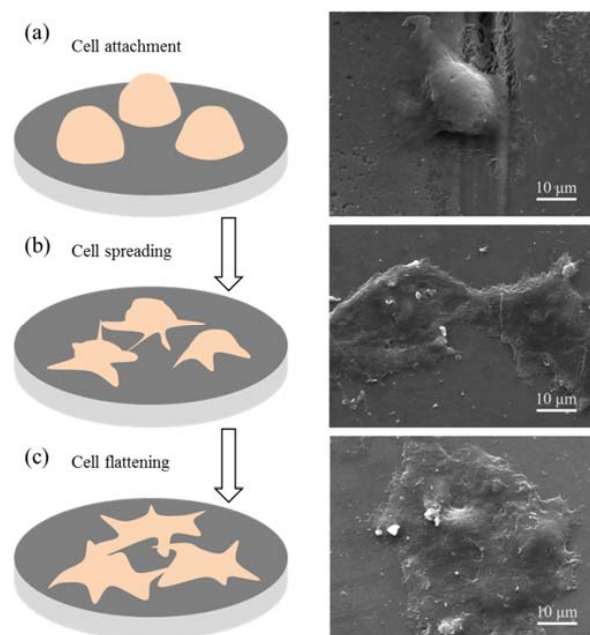


Figure 10. Cell attachment and spreading on the scaffolds: (a) attachment, (b) spreading and (c) flattening (left: graphical representation and right: micrographs).

4. Conclusions

In this paper, the mechanically strong CaSiO₃ scaffolds were fabricated by incorporating B₂O₃-ZnO liquid phase. The liquid phase improved the microstructures and densification of the scaffolds. When the weight ratio of B₂O₃ to ZnO was 35:65, the fracture toughness and compressive strength reached optimized values, namely $1.57 \pm 0.15 \text{ MPa}\cdot\text{m}^{1/2}$ and $40.69 \pm 1.54 \text{ MPa}$, respectively. The fracture toughness and compressive strength were increased by 48% and 141%, respectively, compared with the scaffolds without liquid phase. Meanwhile, the scaffolds with the liquid phase showed an excellent HAp formation ability and a steady mechanical strength in SBF. Moreover, they were also favorable for cell adhesion and proliferation. Therefore, the utilization of CaSiO₃ scaffolds with B₂O₃-ZnO liquid phase in bone tissue regeneration is promising.

Acknowledgments: This work was supported by the following funds: (1) The Natural Science Foundation of China (51575537, 81572577); (2) Overseas, Hong Kong & Macao Scholars Collaborated Researching Fund of National Natural Science Foundation of China (81428018); (3) Hunan Provincial Natural Science Foundation of China (14JJ1006, 2016JJ1027); (4) The Project of Innovation-driven Plan of Central South University (2015CX008, 2016CX023); (5) The Open-End Fund for the Valuable and Precision Instruments of Central South University; (6) The fund of the State Key Laboratory of Solidification Processing in NWPU (SKLSP201605); (7) The fund of the State Key Laboratory for Powder Metallurgy; (8) The Fundamental Research Funds for the Central Universities of Central South University.

Author Contributions: Songlin Duan, Chengde Gao, Youwen Yang and Long Liu manufactured the scaffold and tested the mechanical performances under the guidance of Cijun Shuai, the structural characterization of the scaffold under the guidance of Cijun Shuai, Fulai Yuan, Sheng Yang, and Pei Feng, the biological test of the scaffold under the guidance of Dao Gao. All authors discussed the result and approved the final manuscript.

Conflicts of Interest: The authors declare no conflict of interest.

References

1. Salinas, A.J.; Vallet-Regí, M. Bioactive ceramics: From bone grafts to tissue engineering. *RSC Adv.* **2013**, *3*, 11116–11131. [[CrossRef](#)]
2. Gandolfi, M.G.; Ciapetti, G.; Taddei, P.; Perut, F.; Tinti, A.; Cardoso, M.V.; Van, M.B.; Prati, C. Apatite formation on bioactive calcium-silicate cements for dentistry affects surface topography and human marrow stromal cells proliferation. *Dent. Mater.* **2010**, *26*, 974–992. [[CrossRef](#)] [[PubMed](#)]
3. Lee, Y.C.; Chen, C.; Tsai, X.T. Visualizing the Knowledge Domain of Nanoparticle Drug Delivery Technologies: A Scientometric Review. *Appl. Sci.* **2016**, *6*, 11. [[CrossRef](#)]
4. Ni, S.; Chang, J.; Chou, L. A novel bioactive porous CaSiO₃ scaffold for bone tissue engineering. *J. Biomed. Mater. Res. A* **2006**, *76*, 196–205. [[CrossRef](#)] [[PubMed](#)]
5. Mehrali, M.; Shirazi, S.F.S.; Baradaran, S.; Mehrali, M.; Metselaar, H.S.C.; Kadri, N.A.B.; Osman, N.A.A. Facile synthesis of calcium silicate hydrate using sodium dodecyl sulfate as a surfactant assisted by ultrasonic irradiation. *Ultrason. Sonochem.* **2014**, *21*, 735–742. [[CrossRef](#)] [[PubMed](#)]
6. Mehrali, M.; Moghaddam, E.; Shirazi, S.F.S.; Baradaran, S.; Mehrali, M.; Latibari, S.T.; Metselaar, H.S.C.; Kadri, N.A.; Zandi, K.; Osman, N.A.A. Synthesis, mechanical properties, and in vitro biocompatibility with osteoblasts of calcium silicate-reduced graphene oxide composites. *ACS Appl. Mater. Interfaces* **2014**, *6*, 3947–3962. [[CrossRef](#)] [[PubMed](#)]
7. Zhao, L.; Wu, C.; Lin, K.; Chang, J. The effect of poly(lactic-co-glycolic acid) (PLGA) coating on the mechanical, biodegradable, bioactive properties and drug release of porous calcium silicate scaffolds. *Biomed. Mater. Eng.* **2012**, *22*, 289–300. [[PubMed](#)]
8. Vladescu, A.; Birlik, I.; Braic, V.; Toparli, M.; Celik, E.; Azem, F.A. Enhancement of the mechanical properties of hydroxyapatite by SiC addition. *J. Mech. Behav. Biomed. Mater.* **2014**, *40*, 362–368. [[CrossRef](#)] [[PubMed](#)]
9. Kantana, W.; Jarupoom, P.; Pengpat, K.; Eitssayeam, S.; Tunkasiri, T.; Rujijanagul, G. Properties of hydroxyapatite/zirconium oxide nanocomposites. *Ceram. Int.* **2013**, *39*, S379–S382. [[CrossRef](#)]
10. Shirazi, F.S.; Mehrali, M.; Oshkour, A.A.; Metselaar, H.S.C.; Kadri, N.A.; Osman, N.A.A. Mechanical and physical properties of calcium silicate/alumina composite for biomedical engineering applications. *J. Mech. Behav. Biomed. Mater.* **2014**, *30*, 168–175. [[CrossRef](#)] [[PubMed](#)]

11. Ahmed, A.A.; Ali, A.A.; Mahmoud, D.A.R.; El-Fiqi, A.M. Preparation and characterization of antibacterial P_2O_5 -CaO-Na₂O-Ag₂O glasses. *J. Biomed. Mater. Res. A* **2011**, *98*, 132–142. [[CrossRef](#)] [[PubMed](#)]
12. Kalantar-zadeh, K.; Ou, J.Z.; Daeneke, T.; Mitchell, A.; Sasaki, T.; Fuhrer, M.S. Two dimensional and layered transition metal oxides. *Appl. Mater. Today* **2016**, *5*, 73–89. [[CrossRef](#)]
13. Aly, I.H.M.; Mohammed, L.A.A.; Al-Meer, S.; Elsaid, K.; Barakat, N.A.M. Preparation and characterization of wollastonite/titanium oxide nanofiber bioceramic composite as a future implant material. *Ceram. Int.* **2016**, *42*, 11525–11534. [[CrossRef](#)]
14. Bewerse, C.; Brinson, L.C.; Dunand, D.C. NiTi with 3D-interconnected microchannels produced by liquid phase sintering and electrochemical dissolution of steel tubes. *J. Mater. Process. Technol.* **2014**, *214*, 1895–1899. [[CrossRef](#)]
15. Lin, K.; Chang, J.; Liu, Z.; Zeng, Y.; Shen, R. Fabrication and characterization of 45S5 bioglass reinforced macroporous calcium silicate bioceramics. *J. Eur. Ceram. Soc.* **2009**, *29*, 2937–2943. [[CrossRef](#)]
16. Parkhomey, O.; Pinchuk, N.; Sych, O.; Tomila, T.; Kuda, O.; Tovstonoh, H.; Gorban', V.; Kolesnichenko, V.; Yan, E. Effect of particle size of starting materials on the structure and properties of biogenic hydroxyapatite/glass composites. *Process. Appl. Ceram.* **2016**, *10*, 1–8. [[CrossRef](#)]
17. Silva, M.J.D.; Bartolomé, J.F.; Aza, A.H.D.; Mello-Castanho, S. Glass ceramic sealants belonging to BAS (BaO-Al₂O₃-SiO₂) ternary system modified with B₂O₃ addition: A different approach to access the SOFC seal issue. *J. Eur. Ceram. Soc.* **2016**, *36*, 631–644. [[CrossRef](#)]
18. Wang, X.; Zhang, L.; Ke, X.; Wang, J.; Yang, G.; Yang, X.; He, D.; Shao, H.; He, Y.; Fu, J. 45S5 Bioglass analogue reinforced akermanite ceramic favorable for additive manufacturing mechanically strong scaffolds. *RSC Adv.* **2015**, *5*, 102727–102735. [[CrossRef](#)]
19. Yang, X.; Zhang, L.; Chen, X.; Sun, X.; Yang, G.; Guo, X.; Yang, H.; Gao, C.; Gou, Z. Incorporation of B₂O₃ in CaO-SiO₂-P₂O₅ bioactive glass system for improving strength of low-temperature co-fired porous glass ceramics. *J. Non-Cryst. Solids* **2012**, *358*, 1171–1179. [[CrossRef](#)]
20. Dzondogadet, M.; Mayapnzietchueng, R.; Hess, K.; Nabet, P.; Belleville, F.; Dousset, B. Action of boron at the molecular level. *Biol. Trace Elem. Res.* **2002**, *85*, 23–33. [[CrossRef](#)]
21. Hakki, S.S.; Bozkurt, B.S.; Hakki, E.E. Boron regulates mineralized tissue-associated proteins in osteoblasts (MC3T3-E1). *J. Trace Elem. Med. Biol.* **2010**, *24*, 243–250. [[CrossRef](#)] [[PubMed](#)]
22. Carbajal, L.; Serena, S.; Caballero, A.; Saínz, M.A.; Detsch, R.; Boccaccini, A.R. Role of ZnO additions on the β/α phase relation in TCP based materials: Phase stability, properties, dissolution and biological response. *J. Eur. Ceram. Soc.* **2014**, *34*, 1375–1385. [[CrossRef](#)]
23. Ito, A.; Kawamura, H.; Otsuka, M.; Ikeuchi, M.; Ohgushi, H.; Ishikawa, K.; Onuma, K.; Kanzaki, N.; Yu, S.; Ichinose, N. Zinc-releasing calcium phosphate for stimulating bone formation. *Mater. Sci. Eng. C* **2002**, *22*, 21–25. [[CrossRef](#)]
24. Pan, Y.J.; Lin, J.H.; Chiang, K.C. Biomedical Applications of Antibacterial Nanofiber Mats Made of Electrospinning with Wire Electrodes. *Appl. Sci.* **2016**, *6*, 46. [[CrossRef](#)]
25. Minaev, V.S.; Petrova, V.Z.; Timoshenkov, S.P.; Khafizov, R.R.; Sharagov, V.A. Glass Formation and glass-forming ability of melts in AlIO-B₂O₃ binary systems (AlIO = BeO, MgO, CaO, SrO, BaO, ZnO, CdO). *Glass Phys. Chem.* **2004**, *30*, 215–225. [[CrossRef](#)]
26. Shuai, C.; Gao, C.; Nie, Y.; Hu, H.; Qu, H.; Peng, S. Structural design and experimental analysis of a selective laser sintering system with nano-hydroxyapatite powder. *J. Biomed. Nanotechnol.* **2010**, *6*, 370–374. [[CrossRef](#)] [[PubMed](#)]
27. Duan, S.; Feng, P.; Gao, C.; Xiao, T.; Yu, K.; Shuai, C.; Peng, S. Microstructure evolution and mechanical properties improvement in liquid-phase-sintered hydroxyapatite by laser sintering. *Materials* **2015**, *8*, 1162–1175. [[CrossRef](#)]
28. Kokubo, T.; Kushitani, H.; Sakka, S.; Kitsugi, T.; Yamamuro, T. Solutions able to reproduce in vivo surface-structure changes in bioactive glass-ceramic A-W3. *J. Biomed. Mater. Res.* **1990**, *24*, 721–734. [[CrossRef](#)] [[PubMed](#)]
29. Murphy, C.M.; O'Brien, F.J. Understanding the effect of mean pore size on cell activity in collagen-glycosaminoglycan scaffolds. *Cell Adhes. Migr.* **2010**, *4*, 377–381. [[CrossRef](#)]
30. Fedorovich, N.E.; Alblas, J.; Hennink, W.E.; Öner, F.C.; Dhert, W.J.A. Organ printing: The future of bone regeneration? *Trends Biotechnol.* **2011**, *29*, 601–606. [[CrossRef](#)] [[PubMed](#)]

31. Yu, H.; Ning, C.; Lin, K.; Chen, L. Preparation and characterization of PLLA/CaSiO₃/apatite composite films. *Int. J. Appl. Ceram. Technol.* **2012**, *9*, 133–142. [[CrossRef](#)]
32. Ni, S.; Lin, K.; Chang, J.; Chou, L. Beta-CaSiO₃/beta-Ca₃(PO₄)₂ composite materials for hard tissue repair: In vitro studies. *J. Biomed. Mater. Res. A* **2008**, *85*, 72–82. [[CrossRef](#)] [[PubMed](#)]



© 2017 by the authors. Licensee MDPI, Basel, Switzerland. This article is an open access article distributed under the terms and conditions of the Creative Commons Attribution (CC BY) license (<http://creativecommons.org/licenses/by/4.0/>).